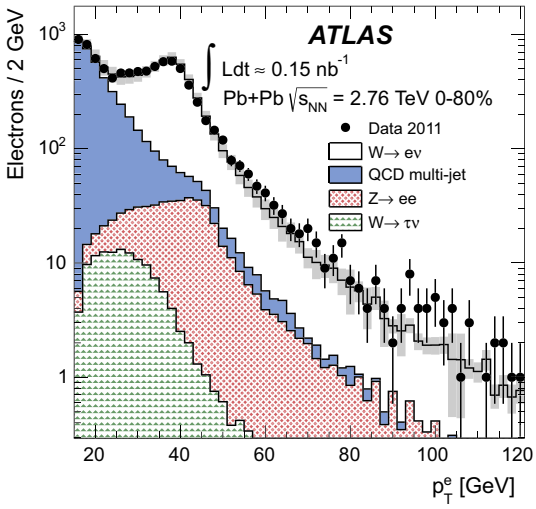

Fig. 4 Electron transverse momentum distribution in the data (*points*). The p_{T} distribution of multi-jet events from a data control sample (see text) and of simulated electroweak processes ($W \to \tau\nu_\tau$ and $Z \to e^+e^-$) are also shown. The total uncertainties from the fit are shown as *solid grey bands*

7 Yield correction procedure

In order to correct the data for losses attributable to the trigger, reconstruction, and selection efficiencies, a correction factor is applied to the measured yields after background subtraction. This correction factor $C_{W^\pm}$ is defined by the following ratio:

$$C_{W^\pm} = \frac{N_W^{\mathrm{rec}}}{N_W^{\mathrm{gen,fid}}}, \tag{4}$$

where N_W^{rec} represents the number of $W \to \ell\nu_\ell$ events reconstructed in the fiducial region and satisfying final selection criteria, and $N_W^{\mathrm{gen,fid}}$ signifies the number of $W \to \ell\nu_\ell$ events in the same phase space at the generator-level. This is calculated separately for each charge, $|\eta_\ell|$ interval, and centrality class. The denominator in Eq. (4) is evaluated directly from the boson decay i.e. Born level; this way of constructing the correction factor accounts for effects due to migration and QED radiation in the final state. Corrections for reconstruction and selection are derived solely from the signal MC simulation, whereas the trigger efficiencies are obtained from the data in each $|\eta_\ell|$ interval and centrality class.

In both the muon and electron channels, the $C_{W^\pm}$ significantly depends on the event centrality and $|\eta_\ell|$. In the muon channel, the integrated $C_{W^\pm}$ is (67.4 ± 0.2) %, ranging from 32 % in the most central events in the highest $|\eta_\mu|$ region to 85 % in the most peripheral events at mid-pseudorapidity. In the electron channel, the integrated $C_{W^\pm}$ is (39.2 ± 0.3) %, ranging from 34 % in the most central events to 51 % in the most peripheral centrality class. The large variations in the $C_{W^\pm}$ are attributable to two main factors: areas of the detector with limited coverage and the centrality dependence of the isolation efficiency and $p_{\mathrm{T}}^{\mathrm{miss}}$ resolution.

The differential W boson production yields in the fiducial region are computed as:

$$N_{W^\pm}(|\eta_\ell|, \text{centrality}) = \frac{N_{W^\pm}^{\mathrm{obs}} - N^{\mathrm{bkg}}}{C_{W^\pm}}, \tag{5}$$

where $N_{W^\pm}^{\mathrm{obs}}$ signifies the number of candidate events observed in the data and N^{bkg} the number of background events in a given $|\eta_\ell|$ and centrality class.

The combination of the results from each channel are reported both as an integrated result in each centrality class and as a differential measurement as a function of $|\eta_\ell|$. The integrated result requires the extrapolation of each measurement to the full pseudorapidity region, $|\eta_\ell| < 2.5$ – this includes the excluded regions discussed above. Correction factors for this extrapolation are derived from the signal MC simulation and increase the integrated yield for muons by 7.5 % and electrons by 6.6 %. In the differential measurement as a function of $|\eta_\ell|$, the extrapolation is performed only in the most forward bin up to $|\eta_\ell| = 2.5$. The correction increases the number of signal candidates in this bin by 28 % in the muon channel and 7 % in the electron channel.

8 Systematic uncertainties

The systematic uncertainties are studied separately for each charge, $|\eta_\ell|$, and centrality class. The magnitude by which each uncertainty is correlated from bin-to-bin is determined from the change in the corrected yields as a function of $|\eta_\ell|$ and centrality after applying a systematic variation. The sources of uncertainty considered fully correlated between bins are as follows: the $p_{\mathrm{T}}^{\mathrm{miss}}$ resolution, electroweak and QCD multi-jet background estimations, lepton isolation efficiencies, lepton and track reconstruction efficiencies, lepton energy/momentum scales and resolutions, extrapolation corrections and $\langle N_{\mathrm{coll}} \rangle$. The dominant systematic uncertainty in both channels originates from the missing transverse momentum resolution. In the asymmetry and charge ratio measurements, uncertainties correlated between charges largely cancel. This correlation is determined for each source of systematic uncertainty from the variation in the charge ratio measurements with respect to the nominal values.

8.1 Muon channel

The resolution on the $p_{\mathrm{T}}^{\mathrm{miss}}$ (described in Sect. 4) worsens with an increasing soft particle contribution to the vector sum of Eq. (2). This in turn depends on the lower track p_{T} threshold. The variation in the resolution with lower track p_{T}

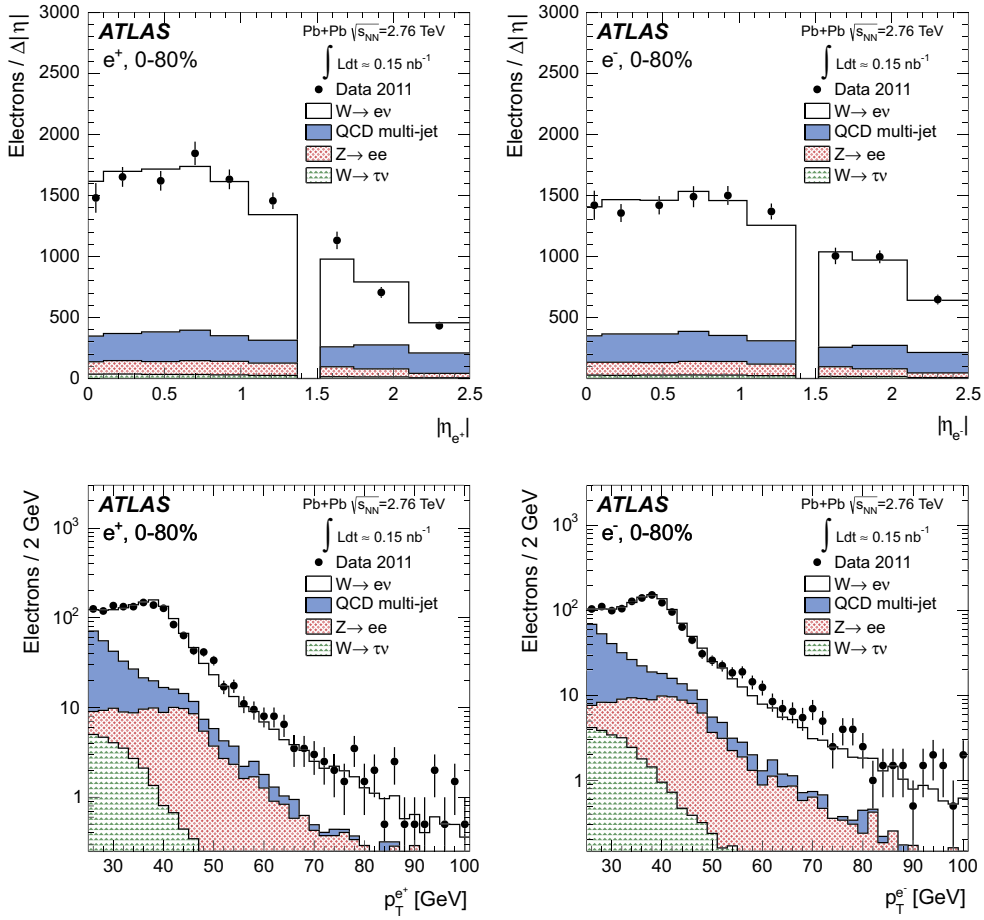

Fig. 5 Measured electron absolute pseudorapidity (*top*) and transverse momentum (*bottom*) distributions for $W^+ \rightarrow e^+\nu_e$ (*left*) and $W^- \rightarrow e^-\bar{\nu}_e$ (*right*) candidates after applying the complete set of selection requirements in the fiducial region, $p_{\mathrm{T}}^{e} > 25$ GeV, $p_{\mathrm{T}}^{\mathrm{miss}} > 25$ GeV, $m_{\mathrm{T}} > 40$ GeV and $|\eta_e| < 2.47$ excluding the transition region ($1.37 < |\eta_e| < 1.52$). The contributions from electroweak and QCD multi-jet processes are normalised according to their expected number of events. The $W \rightarrow e\nu_e$ MC events are normalised to the number of background-subtracted events in the data. The background and signal predictions are added sequentially

threshold is attributable to sources of spurious $p_{\mathrm{T}}^{\mathrm{miss}}$ – e.g. undetected tracks, limited detector coverage, inactive material, finite detector resolution. These sources become amplified when a larger number of tracks are considered in the vector sum. A larger σ_{miss} in the $p_{\mathrm{T}}^{\mathrm{miss}}$ distribution implies a larger uncertainty of the true neutrino p_{T}. However, setting a lower track p_{T} threshold too high can also introduce sources of fake $p_{\mathrm{T}}^{\mathrm{miss}}$ by vetoing tracks required to balance the transverse energy of the event. Therefore, to optimise the $p_{\mathrm{T}}^{\mathrm{miss}}$ calculation, several lower track p_{T} thresholds were studied in MB events and 3 GeV is considered optimal. To quantify the uncertainty on the optimisation, the p_{T} threshold of the tracks used in Eq. (2) is varied in both data and MC simulation by ± 1 GeV relative to the nominal track p_{T} threshold. All background sources, correction factors, and signal yields are recalculated during this procedure, resulting in an estimated uncertainty in the signal yield of 2.0–4.0 %.

The uncertainty in the QCD multi-jet background estimation arises primarily from the extrapolation procedure. There are two contributing factors: how well the MC simulation represents the shape of the QCD multi-jet muon p_{T} distribution – particularly in the high-p_{T} region – and to what degree this distribution is altered by jet energy-loss in the medium. Both contributions may be accounted for by scaling the muon p_{T} distribution from simulated QCD multi-jet events by a p_{T}-dependent nuclear modification factor. The scale factors are calculated according to the procedure from Ref. [15] and are defined as the ratio of the inclusive charged hadron yield per binary collision in a heavy-ion event and the charged hadron yield in a pp collision. This is performed for each centrality class. Since there is little difference between the nuclear modification factor between heavy-flavour muons and inclusive charged hadrons [15,56], this scaling procedure is a valid estimation of the extrapolation uncertainty. Applying this factor to each muon p_{T} bin results in a maximum

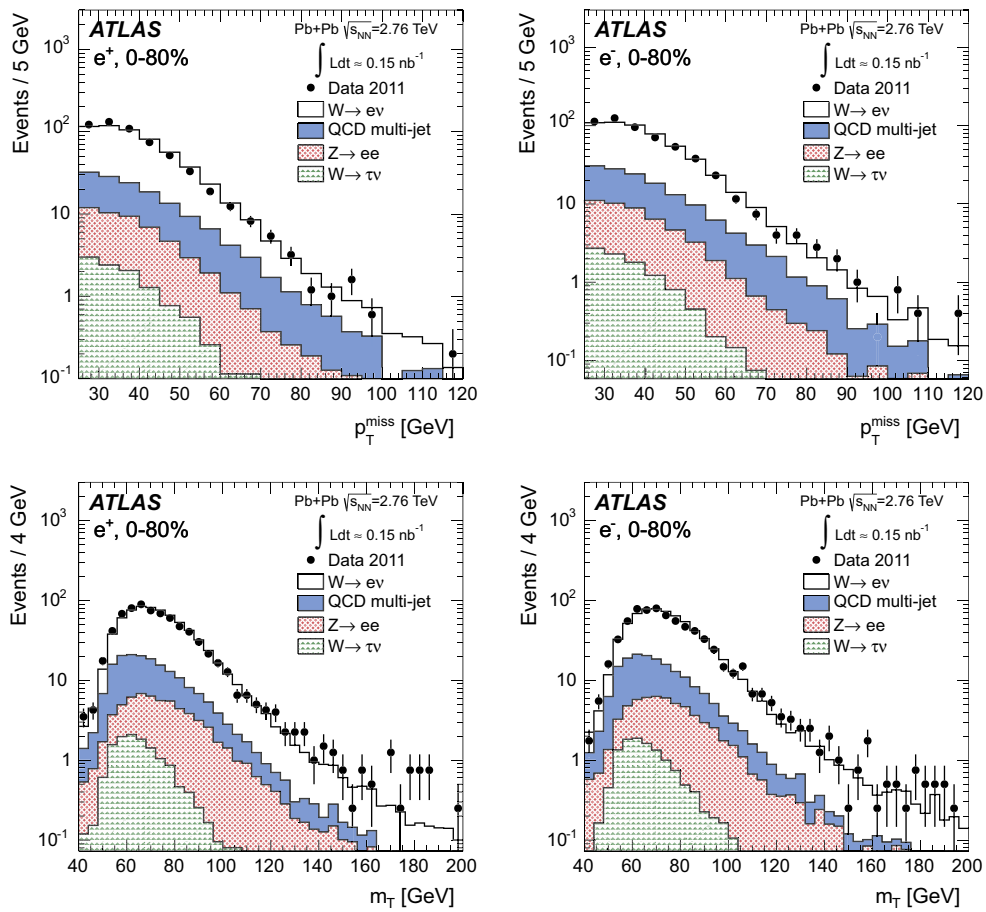

Fig. 6 Measured missing transverse momentum (*top*) and transverse mass (*bottom*) distributions for $W^+ \to e^+\nu_e$ (*left*) and $W^- \to e^-\bar{\nu}_e$ (*right*) candidates after applying the complete set of selection requirements in the fiducial region, $p_{\mathrm{T}}^{e} > 25$ GeV, $p_{\mathrm{T}}^{\mathrm{miss}} > 25$ GeV, $m_{\mathrm{T}} > 40$ GeV and $|\eta_e| < 2.47$ excluding the transition region ($1.37 < |\eta_e| < 1.52$). The contributions from electroweak and QCD multi-jet processes are normalised according to their expected number of events. The $W \to e\nu_e$ MC events are normalised to the number of background-subtracted events in the data. The background and signal predictions are added sequentially

uncertainty in the QCD multi-jet background of 50 % and variations in the final signal yields from 0.4 % to 2.0 %.

The electroweak background uncertainty is estimated separately for $Z \to \mu^+\mu^-$ and $W \to \tau\nu_\tau$. The uncertainty in the Z boson background estimation is determined by scaling the number of Z events in each η_μ interval to the number of events estimated from the MC simulation rather than those observed in the data in each centrality class. The variation in the number of $W \to \mu\nu_\mu$ events in each $|\eta_\mu|$ or centrality class with respect to the nominal yields is < 0.1 %. The systematic error in the τ background estimation is evaluated by assuming that the muon selection efficiencies for the $p_{\mathrm{T}}^{\mathrm{miss}}$ and m_{T} requirements in the $W \to \tau\nu_\tau \to \mu\nu_\mu\nu_\tau\nu_\tau$ sample are identical to those in the $W \to \mu\nu_\mu$ sample for muons with $p_{\mathrm{T}}^{\mu} > 25$ GeV. Estimating the τ background with these efficiencies from the $W \to \mu\nu_\mu$ sample results in a variation in the signal yields no larger than 0.1 % of the nominal number of signal events in the data. Other sources of background from $Z \to \tau\tau$ and $t\bar{t}$ events are also included as a systematic uncertainty and result in a signal variation of less than 0.2 %.

A systematic uncertainty attributable to the modelling accuracy of the isolation in the MC simulation is assessed by varying the ΔR and $\sum p_{\mathrm{T}}^{\mathrm{ID}}$ requirements in both data and simulation. This uncertainty is estimated by re-evaluating the yields either with a larger ΔR or a larger $\sum p_{\mathrm{T}}^{\mathrm{ID}}$. The ΔR around the muon momentum direction is increased from 0.2 to 0.3, and the requirement on the $\sum p_{\mathrm{T}}^{\mathrm{ID}}$ is increased from 10 % to 20 % of the muon p_{T}. This results in a yield variation of 1–2 % in each centrality, $|\eta_\mu|$, or charge class.

Systematic uncertainties related to the $C_{W^\pm}$ correction originate from uncertainties in the muon p_{T} resolution, reconstruction efficiency, and trigger efficiency. These uncertainties were previously evaluated for the 2011 heavy-ion data-taking period in Ref. [22]. A short summary of the

methodology used in estimating these uncertainties and their respective contributions to the W analysis is provided below. An uncertainty in the muon p_T resolution due to differences in the detector performance in simulation relative to actual data-taking conditions is estimated by additionally smearing the p_T of muons in the MC simulation in the range allowed by the systematic uncertainties in Ref. [57]. The correction factors are then re-evaluated, and the yield variation is used as the systematic uncertainty. The relative uncertainty from this procedure results in a variation of less than 1.0 % in the number of signal events in each η_μ, centrality, and charge class. Uncertainties in the muon reconstruction efficiency are also estimated from $Z \to \mu^+\mu^-$ events. To estimate this uncertainty, $Z \to \mu^+\mu^-$ MC events are re-weighted such that the ratio of the number of muon pairs reconstructed using both the ID and MS components and muon pairs reconstructed using only the MS component – with no restriction on the ID component – agree in data and the MC simulation. The reconstruction efficiencies in the MC simulation are then recalculated and result in an additional 1.0 % uncertainty in the number of $W \to \mu\nu_\mu$ events. Uncertainties in the muon trigger efficiency are determined from differences in the efficiencies calculated using single muons from MB events and a tag-and-probe method applied to a $Z \to \mu^+\mu^-$ sample. This results in yield variations of 0.4 %.

Scaling uncertainties in $\langle N_{\text{coll}} \rangle$ are also applied when reporting the yields per binary collision. These were shown in Table 2 and arise from possible contamination due to photonuclear events and diffractive processes. The procedure for calculating these uncertainties is described in detail in Ref. [49]. This uncertainty is largest in the most peripheral events and amounts to 9.4 %. Integrated over all events the $\langle N_{\text{coll}} \rangle$ uncertainty is around 8.5 %.

The extrapolation of the yields over $|\eta_\mu| < 2.5$ also introduces a source of systematic uncertainty. This uncertainty is mainly attributable to the PDF uncertainty, which has been studied extensively in pp collisions at the LHC by ATLAS [26] using the same PDF set that this analysis uses to correct the data. The uncertainties are derived from differences in the correction factor using various PDF sets, differences due to the parton-shower modelling, and the PDF error eigenvectors. These individual contributions are added in quadrature and result in uncertainties at the 0.2 % level. An uncertainty of 0.3 % is associated with the differential production measurement in the highest $|\eta_\mu|$ bin.

Table 3 presents a summary of the maximum values for all systematic uncertainties included in the muon channel. Systematic uncertainties correlated between different centrality or $|\eta_\mu|$ intervals are 3–5 %. The bin-uncorrelated systematic uncertainties, which are comprised of statistical uncertainties from the background estimation, trigger efficiency, and correction factors, are 1–3 %. These are also included at the bottom of Table 3.

Table 3 Maximum values of the relative systematic uncertainties in the $W \to \mu\nu_\mu$ channel on the measured event yield in each $|\eta_\mu|$ interval and centrality class. Correlated uncertainties represent those that are correlated as a function of centrality or $|\eta_\mu|$. Bin-uncorrelated uncertainties represent statistical uncertainties in the background estimation, trigger efficiencies, and yield correction factors

Source	Uncertainty [%]
p_T^{miss} resolution	4.0
QCD multi-jet background	2.0
Electroweak + $t\bar{t}$ backgrounds	0.2
Muon isolation	2.0
Muon reconstruction	1.0
Muon p_T resolution	1.0
Muon trigger efficiency	0.4
Extrapolation correction	0.3
Total bin-correlated	5.2
$\langle N_{\text{coll}} \rangle$ determination	9.4
Total bin-uncorrelated	3.0

8.2 Electron channel

In the electron channel, the contribution due to the missing transverse momentum resolution is evaluated using the same procedure as in the muon channel. The yield variation is on average 2–5 % with a maximum deviation of 10 %.

The uncertainty in the QCD multi-jet background estimation arises from the choice of control region used to model the p_T spectrum of fake electrons from QCD multi-jet processes. This uncertainty is assessed by modifying the background composition of the control region in order to test the stability in the fitting procedure under shape changes. In addition, the constraint on the azimuthal separation between a jet – reconstructed at the EM scale with $E_T > 25$ GeV – and the p_T^{miss} vector is loosened or tightened [54]. After applying these modifications, the altered background fractions result in signal yield variations below 5 %.

The systematic contribution associated with the electron isolation is evaluated by varying the isolation ratio from 0.2 to 0.3. This results in an average corrected yield variation of 2 % with a maximum variation of 4 %.

Systematic uncertainties in the electroweak background estimations are obtained from the 5 % theoretical uncertainty on each of the W and Z boson production cross-sections. These uncertainties are treated as fully correlated among various W and Z boson production processes. The resulting relative systematic uncertainty is approximately 0.2 % with the largest deviation at the level of 0.5 %.

The main uncertainty associated with the $C_{W^\pm}$ correction stems from possible discrepancies between data and MC simulation. In general, there are two contributions to this discrepancy: differences in the detector performance description and shortcomings in the physics model of the MC simulation

that lead to distortions in the $C_{W^\pm}$ correction given the finite binning used. To account for the first contribution, a result obtained in pp collisions [54] is used. There it was found that the electron identification efficiencies in the data are consistent with those from the MC simulation within a 3 % total relative uncertainty, which is applied as a systematic uncertainty for this analysis. The second contribution is estimated by re-weighting the signal MC sample such that the $|\eta_e|$ distribution in the simulation matches the one measured in the data. This systematic variation results in an average relative systematic uncertainty below 1 %.

The electron trigger efficiency obtained from the data using a tag-and-probe method is compared to the efficiency from MC simulation. The efficiencies from both samples are consistent within their statistical uncertainties. The statistical errors in the data are propagated as uncertainties on the event yield, introducing a 0.2 % uncertainty.

The systematic uncertainty due to the extrapolation of the yields in the region $|\eta_e| < 2.5$ is attributed to the same factors as in the muon channel (i.e. PDF uncertainties). This introduces an additional 0.2 % uncertainty in the yields from the extrapolated $|\eta_e|$ regions. A 0.1 % uncertainty is associated with the differential production measurement in the highest $|\eta_e|$ bin.

The charge of leptons from $W \to e\nu_e$ decays may be misidentified, resulting in possible misrepresentations of charge-dependent observables. The charge misidentification probability is determined from the signal MC sample. It is below 0.2 % for $|\eta_e| < 1.37$ and between 1–3 % in the highest $|\eta_e|$ region. These values are consistent with data-driven measurements [55] except in the highest $|\eta_e|$ bin, where a disagreement at the level of 50 % is found. This percentage is propagated as an uncertainty in the difference between the correction factors of each charge, resulting in a systematic uncertainty of 1.5 % and 2.0 % in the number of W^- and W^+ boson yields, respectively, in the highest $|\eta_e|$ bin. In all other $|\eta_e|$ regions, the average relative systematic uncertainty is below 1 %. The uncertainty in the charge asymmetry measurement is determined by varying the W^- and W^+ boson yields by their respective uncertainties in opposite directions.

Table 4 presents a summary of the maximum values for all systematic uncertainties considered in the electron channel. The bin-correlated systematic uncertainties among different centrality or $|\eta_e|$ bins are 4.0–10.5 %. The bin-uncorrelated systematic uncertainties, which are comprised of statistical uncertainties from the background estimation, trigger efficiency, and correction factors, are 3.0–5.8 %. These are summarised at the bottom of Table 4.

Table 4 Maximum values of the relative systematic uncertainties in the $W \to e\nu_e$ channel on the measured event yield in each $|\eta_e|$ interval and centrality class. Correlated uncertainties represent those that are correlated as a function of centrality or $|\eta_e|$. Uncorrelated uncertainties represent statistical uncertainties in the background estimation, trigger efficiencies, and yield correction factors

Source	Uncertainty [%]
$p_{\mathrm{T}}^{\mathrm{miss}}$ resolution	10.0
QCD multi-jet background	5.0
Electroweak backgrounds	0.5
Electron isolation	4.0
Electron reconstruction	3.2
Electron trigger efficiency	0.2
Charge misidentification	2.0
Extrapolation correction	0.2
Total bin-correlated	10.5
$\langle N_{\mathrm{coll}} \rangle$ determination	9.4
Total bin-uncorrelated	5.8

8.3 Channel combination

The results from the $W \to \mu\nu_\mu$ and $W \to e\nu_e$ channels are combined in order to increase the precision of the measurement. Although the two channels share a common kinematic phase space, differences in their geometrical acceptances must be considered in the combination procedure. After verifying that the results are compatible, the two channels are combined using an averaging method with weights proportional to the inverse square of the individual uncertainties. Uncertainties treated as fully correlated between the muon and electron channels include the $p_{\mathrm{T}}^{\mathrm{miss}}$ resolution, electroweak background subtraction, and $\langle N_{\mathrm{coll}} \rangle$. All other sources are treated as uncorrelated.

8.4 Theoretical predictions

Uncertainties inherent in the PDF and EPS09 nuclear corrections are evaluated using the Hessian method to quantify the relative differences between current experimental uncertainties and central values of the PDF [58]. PDF uncertainties in the Pb nucleus are obtained from the weighted average of free proton and neutron PDF uncertainties. In addition, uncertainties in the renormalisation and factorisation scales are also taken into account by increasing and decreasing each scale by a factor of two and using the maximum variation as the uncertainty in each bin.

9 Results

The total number of background-subtracted and efficiency-corrected events in the fiducial phase space ($p_{\mathrm{T}}^{\ell} > 25$ GeV, $p_{\mathrm{T}}^{\mathrm{miss}} > 25$ GeV, $m_{\mathrm{T}} > 40$ GeV) and after extrapolation to $|\eta_\ell| < 2.5$ is presented in Table 5 along with the ratio of W^+ and W^- boson production.

Table 5 Summary of the number of background-subtracted and efficiency-corrected events for $W \to \mu\nu_\mu$ and $W \to e\nu_e$ events. The yields are defined in a fiducial region $p_T^\ell > 25$ GeV, $p_T^{miss} > 25$ GeV, $m_T > 40$ GeV and are extrapolated to $|\eta_\ell| < 2.5$

	$W \to \mu\nu_\mu$
W^+	5870 ± 100 (stat.) ± 90 (syst.)
W^-	5680 ± 100 (stat.) ± 80 (syst.)
W^+/W^-	1.03 ± 0.03 (stat.) ± 0.02 (syst.)
	$W \to e\nu_e$
W^+	5760 ± 150 (stat.) ± 90 (syst.)
W^-	5650 ± 150 (stat.) ± 110 (syst.)
W^+/W^-	1.02 ± 0.04 (stat.) ± 0.01 (syst.)

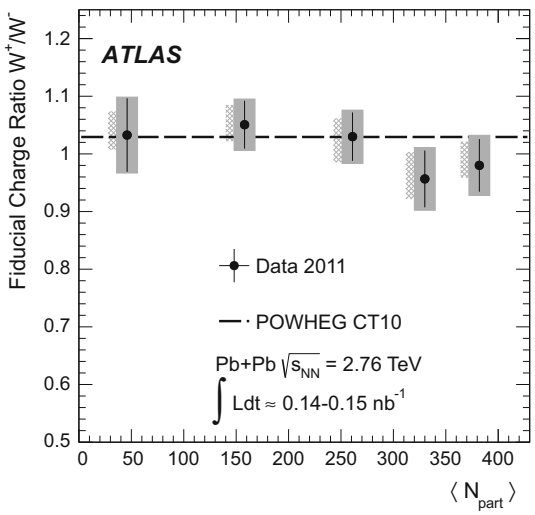

Fig. 7 Ratio of W^+ and W^- candidates (from $W \to \ell\nu_\ell$) as a function of $\langle N_{part}\rangle$. The kinematic requirements are $p_T^\ell > 25$ GeV, $p_T^{miss} > 25$ GeV, $m_T > 40$ GeV, and $|\eta_\ell| < 2.5$. Also shown is a QCD NLO prediction from POWHEG. Statistical uncertainties are shown as *black bars*. The *filled grey boxes* represent statistical and bin-uncorrelated systematic uncertainties added in quadrature, whereas the *grey-hatched boxes* represent bin-correlated uncertainties and are offset for clarity

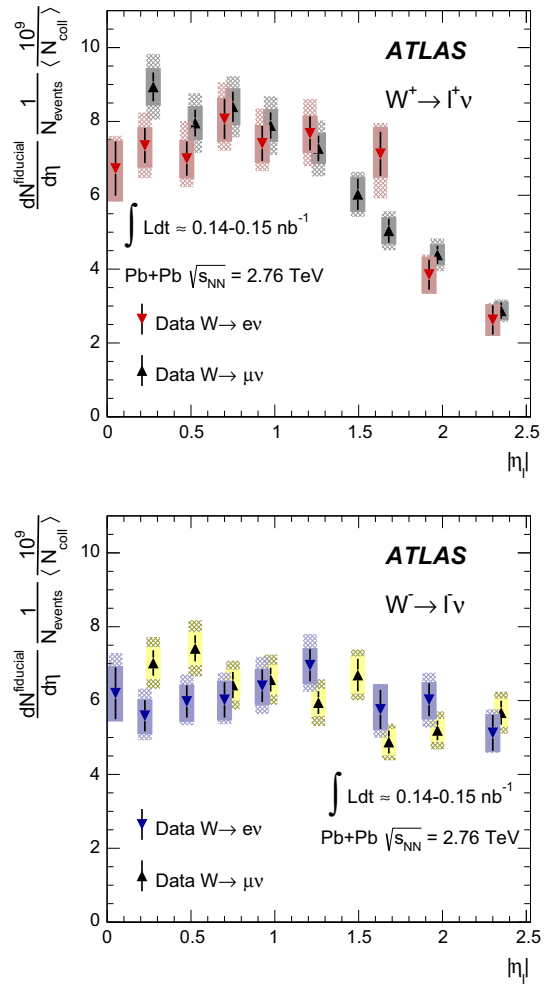

Fig. 8 Differential production yields per binary collision for W^+ (*top*) and W^- (*bottom*) events from electron and muon channels. Due to acceptance the first bin in the muon channel and the seventh bin in the electron channel are not covered. Muon points are shifted horizontally for visibility. The kinematic requirements are $p_T^\ell > 25$ GeV, $p_T^{miss} > 25$ GeV, and $m_T > 40$ GeV. Statistical errors are shown as *black bars*, whereas bin-uncorrelated systematic and statistical uncertainties added in quadrature are shown as the *filled error box*. Bin-correlated uncertainties are shown as the *hatched boxes*. These include uncertainties from $\langle N_{coll}\rangle$

The corrected yields from each channel are consistent. Moreover, the contributions from nn and pn collisions are evident. Proton-proton collisions alone would result in a ratio of W^+ and W^- bosons significantly above unity, but in Pb+Pb collisions, the larger number of d valence quarks in the neutron increases W^- production, driving the ratio closer to one. This is supported by Fig. 7, which presents the fiducial charge ratio as a function of $\langle N_{part}\rangle$ for the combined muon and electron channels.

Figure 8 shows a comparison between the differential production yields per binary collision for the muon and electron channels, separately, as a function of $|\eta_\ell|$ for W^+ and W^-. A good agreement is found between the two decay modes. In both decay channels, the distribution from W^+ bosons steeply falls at large $|\eta_\ell|$, whereas this is not the case for W^- events. This behaviour is understood and is further discussed below in connection to the charge asymmetry.

Figure 9 presents the W boson production yield per binary collision for each charge separately as well as inclusively as a function of $\langle N_{part}\rangle$ for the combined data. Also shown are comparisons to QCD NLO predictions. The NLO predictions are consistent with the data for both the charge ratio, as shown in Fig. 7, and production yields in Fig. 9.

As with other heavy-ion electroweak boson measurements, W boson production yields per binary nucleon–nucleon collision are independent of centrality. This suggests that the W boson can be used for benchmarking energy-loss

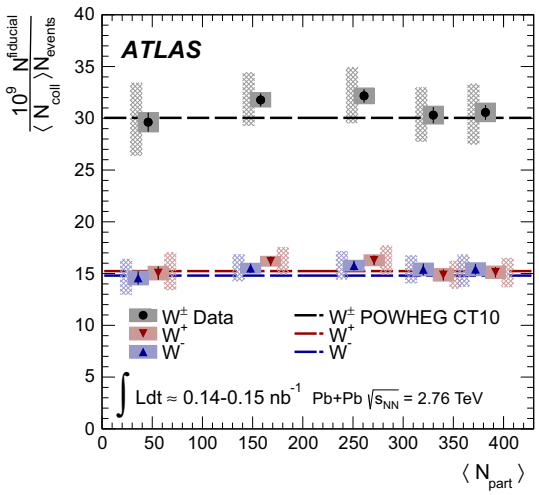

Fig. 9 W boson production yield per binary collision as a function of the mean number of participants $\langle N_{\text{part}} \rangle$ for W^+, W^-, and $W^\pm$ bosons for combined muon and electron channels. The kinematic requirements are $p_{\text{T}}^{\ell} > 25$ GeV, $p_{\text{T}}^{\text{miss}} > 25$ GeV, $m_{\text{T}} > 40$ GeV, and $|\eta_\ell| < 2.5$. Statistical errors are shown as *black bars*, whereas bin-uncorrelated systematic and statistical uncertainties added in quadrature are shown as the *filled error box*. Bin-correlated uncertainties are shown as the *hatched boxes* and are offset for clarity. These include uncertainties from $\langle N_{\text{coll}} \rangle$. Also shown is an NLO QCD prediction

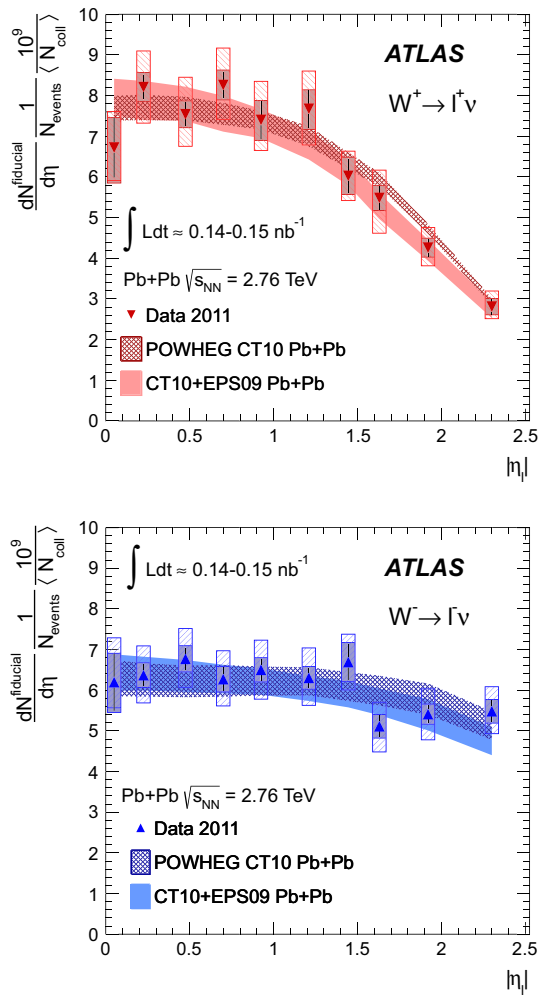

Fig. 10 Differential production yield per binary collision for W^+ (*top*) and W^- (*bottom*) events integrated over all centralities and compared to NLO QCD theoretical predictions with (CT10+EPS09) and without (CT10) nuclear corrections. The kinematic requirements are $p_{\text{T}}^{\ell} > 25$ GeV, $p_{\text{T}}^{\text{miss}} > 25$ GeV, and $m_{\text{T}} > 40$ GeV. Statistical errors are shown as *black bars*, whereas bin-uncorrelated systematic and statistical uncertainties added in quadrature are shown as the *filled error box*. Bin-correlated uncertainties are shown as the *hatched boxes*. These include uncertainties from $\langle N_{\text{coll}} \rangle$. The PDF uncertainties in both the CT10+EPS09 and CT10 predictions are derived from the PDF error eigensets. The total theoretical uncertainty also includes uncertainties in the renormalisation and factorisation scales used in the cross-section calculations

processes in a QGP. Thus, when produced in association with jets, W boson production introduces an additional avenue for exploring in-medium modifications – energy loss due to multiple scattering and gluon radiation – to energetic partons traversing the heavy-ion medium.

Nuclear modifications to the PDF are explored in Figs. 10 and 11, which present the differential $W \to \ell\nu_\ell$ production yields per binary nucleon–nucleon collision and the lepton charge asymmetry, respectively, as a function of $|\eta_\ell|$. Each figure includes NLO predictions with the CT10 PDF set, both with and without EPS09 nuclear corrections. The EPS09 corrections incorporate modifications to the PDF that account for contributions from shadowing, anti-shadowing, the EMC-effect, and Fermi-motion [34].

Both the CT10 and CT10+EPS09 predictions in Figs. 10 and 11 describe the data well. Therefore, at the current level of theoretical and experimental precision, this measurement is insensitive to nuclear modifications to the PDF. Fig. 11 also exhibits a sign-change of the charge asymmetry at $|\eta_\ell| \approx 1.5$, behaviour hitherto only observed at $|\eta_\ell| > 3$ in pp measurements at 7 TeV [26,59]. The negative asymmetry is attributable to the $V - A$ structure of W boson decays, in which the decay angle of the charged lepton is anisotropic and a larger fraction of negatively charged leptons are produced at forward $|\eta_\ell|$. The larger fraction of $W^- \to \ell^-\bar{\nu}_\ell$ events in Pb+Pb compared to pp collisions results in a sign-change of the asymmetry that can be observed within the $|\eta_\ell|$ acceptance of the measurement. This behaviour is in accordance with the NLO QCD predictions.

10 Summary and conclusions

The measurements of $W^\pm$ boson production in Pb+Pb collisions at $\sqrt{s_{\text{NN}}} = 2.76$ TeV are presented using data corresponding to an integrated luminosity of 0.14–0.15 nb^{-1} collected with the ATLAS detector at the LHC. The $W^\pm$

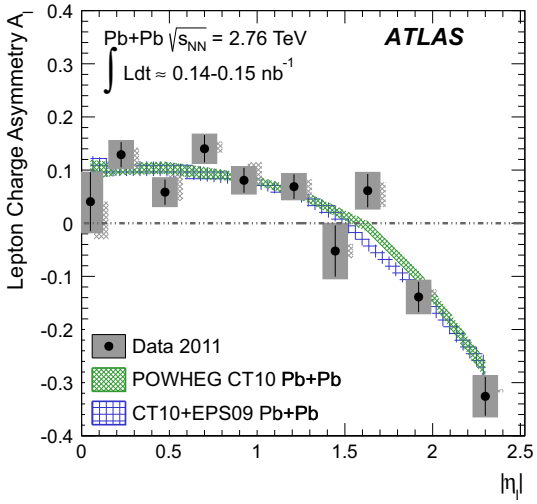

Fig. 11 The lepton charge asymmetry A_ℓ from $W^\pm$ bosons as a function of absolute pseudorapidity compared to theoretical predictions from the CT10 and CT10+EPS09 NLO PDF sets. The kinematic requirements are $p_{\mathrm{T}}^{\ell} > 25$ GeV, $p_{\mathrm{T}}^{\mathrm{miss}} > 25$ GeV, and $m_{\mathrm{T}} > 40$ GeV. Statistical uncertainties are shown as *black bars*, whereas bin-uncorrelated systematic and statistical uncertainties added in quadrature are shown as the *filled error box*. Correlated scaling uncertainties are shown as the *hatched boxes* and are offset for clarity. The PDF uncertainties in both the CT10+EPS09 and CT10 predictions are derived from the PDF error eigensets. The total theoretical uncertainty also includes uncertainties in the renormalisation and factorisation scales used in the cross-section calculations

boson candidates are selected using muons or electrons in the final state in the fiducial region defined by $p_{\mathrm{T}}^{\ell} > 25$ GeV, $p_{\mathrm{T}}^{\mathrm{miss}} > 25$ GeV, $m_{\mathrm{T}} > 40$ GeV and $0.1 < |\eta_\mu| < 2.4$ for muons and $|\eta_e| < 2.47$, excluding the transition region, for electrons. After background subtraction, correction, and extrapolation to a pseudorapidity coverage of $|\eta_\ell| < 2.5$, the numbers of events reported in each channel are consistent.

The W boson production yields are presented as a function of $\langle N_{\mathrm{part}} \rangle$ and $|\eta_\ell|$. These yields, scaled by $1/\langle N_{\mathrm{coll}} \rangle$, are independent of centrality and in agreement with NLO QCD predictions. The lepton charge asymmetry from $W^\pm$ boson decays differs from measurements in pp collisions. This is expected since in Pb+Pb collisions there is an additional neutron component contributing to W boson production. The lepton charge asymmetry agrees well with theoretical predictions using QCD at NLO with CT10 PDF sets with and without EPS09 nuclear corrections. The nuclear corrections account for modifications that are not present in the PDF of free nucleons. However, further improvements in the experimental precision and uncertainties in the theory are needed to establish the existence of nuclear effects. The results presented here clearly indicate that in events associated with a jet, W bosons are an excellent tool for evaluating jet energy-loss in a QGP. Moreover, it was demonstrated that W bosons can be used to study PDFs in multi-nucleon systems. With improved statistical and systematic precision, along with additional data from different colliding systems such as p+Pb, it will be possible to decisively evaluate the extent of nuclear effects on PDFs and to further test theoretical predictions.

Acknowledgments We thank CERN for the very successful operation of the LHC, as well as the support staff from our institutions without whom ATLAS could not be operated efficiently. We acknowledge the support of ANPCyT, Argentina; YerPhI, Armenia; ARC, Australia; BMWFW and FWF, Austria; ANAS, Azerbaijan; SSTC, Belarus; CNPq and FAPESP, Brazil; NSERC, NRC and CFI, Canada; CERN; CONICYT, Chile; CAS, MOST and NSFC, China; COLCIENCIAS, Colombia; MSMT CR, MPO CR and VSC CR, Czech Republic; DNRF, DNSRC and Lundbeck Foundation, Denmark; EPLANET, ERC and NSRF, European Union; IN2P3-CNRS, CEA-DSM/IRFU, France; GNSF, Georgia; BMBF, DFG, HGF, MPG and AvH Foundation, Germany; GSRT and NSRF, Greece; ISF, MINERVA, GIF, I-CORE and Benoziyo Center, Israel; INFN, Italy; MEXT and JSPS, Japan; CNRST, Morocco; FOM and NWO, Netherlands; BRF and RCN, Norway; MNiSW and NCN, Poland; GRICES and FCT, Portugal; MNE/IFA, Romania; MES of Russia and ROSATOM, Russian Federation; JINR; MSTD, Serbia; MSSR, Slovakia; ARRS and MIZŠ, Slovenia; DST/NRF, South Africa; MINECO, Spain; SRC and Wallenberg Foundation, Sweden; SER, SNSF and Cantons of Bern and Geneva, Switzerland; NSC, Taiwan; TAEK, Turkey; STFC, the Royal Society and Leverhulme Trust, United Kingdom; DOE and NSF, United States of America. The crucial computing support from all WLCG partners is acknowledged gratefully, in particular from CERN and the ATLAS Tier-1 facilities at TRIUMF (Canada), NDGF (Denmark, Norway, Sweden), CC-IN2P3 (France), KIT/GridKA (Germany), INFN-CNAF (Italy), NL-T1 (Netherlands), PIC (Spain), ASGC (Taiwan), RAL (UK) and BNL (USA) and in the Tier-2 facilities worldwide.

References

1. I. Arsene et al. [BRAHMS Collaboration], Nucl. Phys. A **757**, 1 (2005). arXiv:nucl-ex/0410020
2. B.B. Back et al. [PHOBOS Collaboration], Nucl. Phys. A **757**, 28 (2005). arXiv:nucl-ex/0410022
3. J. Adams et al. [STAR Collaboration], Nucl. Phys. A **757**, 102 (2005). arXiv:nucl-ex/0501009
4. K. Adcox et al. [PHENIX Collaboration], Nucl. Phys. A **757**, 184 (2005). arXiv:nucl-ex/0410003
5. ATLAS Collaboration, Phys. Lett. B **710**, 363 (2012). arXiv:1108.6027
6. CMS Collaboration, JHEP **1108**, 141 (2011). arXiv:1107.4800
7. M.J. Tannenbaum, Rep. Prog. Phys. **69**, 2005 (2006). arXiv:nucl-ex/0603003
8. B. Mohanty, Nucl. Phys. **A830**, 899C (2009). arXiv:0907.4476
9. K. Fukushima, T. Hatsuda, Rep. Prog. Phys. **74**, 014001 (2011). arXiv:1005.4814
10. B. Mohanty, New J. Phys. **13**, 065031 (2011). arXiv:1102.2495
11. B. Muller, J. Schukraft, B. Wyslouch, Ann. Rev. Nucl. Part. Sci. **62**, 361 (2012). arXiv:1202.3233

12. S.S. Adler et al. [PHENIX Collaboration], Phys. Rev. Lett. **91**, 072301 (2003). arXiv:nucl-ex/0304022
13. J. Adams et al. [STAR Collaboration], Phys. Rev. Lett. **91**, 172302 (2003). arXiv:nucl-ex/0305015
14. K. Aamodt et al. [ALICE Collaboration], Phys. Lett. B **696**, 30 (2011). arXiv:1012.1004
15. CMS Collaboration, Eur. Phys. J. C **72**, 1945 (2012). arXiv:1202.2554
16. ATLAS Collaboration (2014). arXiv:1406.2979
17. ATLAS Collaboration, Phys. Lett. B **719**, 220 (2013). arXiv:1208.1967
18. ATLAS Collaboration, Phys. Rev. Lett. **105**, 252303 (2010). arXiv:1011.6182
19. CMS Collaboration, Phys. Rev. C **84**, 024906 (2011). arXiv:1102.1957
20. CMS Collaboration, Phys. Lett. B **712**, 176 (2012). arXiv:1202.5022
21. S. Afanasiev et al. [PHENIX Collaboration], Phys. Rev. Lett. **109**, 152302 (2012). arXiv:1205.5759
22. ATLAS Collaboration, Phys. Rev. Lett. **110**, 022301 (2013). arXiv:1210.6486
23. CMS Collaboration, Phys. Rev. Lett. **106**, 212301 (2011). arXiv:1102.5435
24. CMS Collaboration, Phys. Lett. B **710**, 256 (2012). arXiv:1201.3093
25. CMS Collaboration, Phys. Lett. B **715**, 66 (2012). arXiv:1205.6334
26. ATLAS Collaboration, Phys. Rev. D **85**, 072004 (2012). arXiv:1109.5141
27. CMS Collaboration, Phys. Rev. Lett. **109**, 111806 (2012). arXiv:1206.2598
28. CMS Collaboration, Phys. Rev. D (2013). arXiv:1312.6283
29. T. Aaltonen et al. [CDF Collaboration], Phys. Rev. Lett. **102**, 181801 (2009). arXiv:0901.2169
30. V. Abazov et al. [D0 Collaboration], Phys. Rev. D **88**, 091102 (2013). arXiv:1309.2591
31. G. Altarelli, R.K. Ellis, G. Martinelli, Nucl. Phys. B **157**, 461 (1979). doi:10.1016/0550-3213(79)90116-0
32. J. Kubar-Andre, F.E. Paige, Phys. Rev. **19**, 221 (1979). doi:10.1103/PhysRevD.19.221
33. J. Kubar, M. Le Bellac, J. Meunier, G. Plaut, Nucl. Phys. B **175**, 251 (1980). doi:10.1016/0550-3213(80)90053-X
34. H. Paukkunen, C.A. Salgado, JHEP **1103**, 071 (2011). We thank the authors for providing us with their EPS09 predictions. arXiv:1010.5392
35. ATLAS Collaboration, JINST **3**, S08003 (2008)
36. ATLAS Collaboration, LHCC-I-016. CERN-LHCC-2007-001. http://cds.cern.ch/record/1009649
37. ATLAS Collaboration, Eur. Phys. J. C **72**, 1849 (2012). arXiv:1110.1530
38. S. Agostinelli et al., Nucl. Instrum. Meth. A **506**, 250 (2003)
39. ATLAS Collaboration, Eur. Phys. J. C **70**, 823 (2010). arXiv:1005.4568
40. X.N. Wang, M. Gyulassy, Phys. Rev. D **44**, 3501 (1991)
41. S. Alioli, P. Nason, C. Oleari, E. Re, JHEP **0807**, 060 (2008). arXiv:0805.4802
42. T. Sjostrand, S. Mrenna, P.Z. Skands, Comput. Phys. Commun. **178**, 852 (2008). arXiv:0710.3820
43. H.-L. Lai et al., Phys. Rev. D **82**, 074024 (2010). arXiv:1007.2241
44. A. Sherstnev, R. Thorne, Eur. Phys. J. C **55**, 553 (2008). arXiv:0711.2473
45. S. Jadach, J.H. Kuhn, Z. Was, Comput. Phys. Commun. **64**, 275 (1990)
46. P. Golonka, Z. Was, Eur. Phys. J. C **45**, 97 (2006). arXiv:hep-ph/0506026
47. ATLAS Collaboration, Phys. Lett. B **707**, 330 (2012). arXiv:1108.6018
48. ATLAS Collaboration, ATLAS-CONF-2012-122. http://cds.cern.ch/record/1473425
49. M.L. Miller, K. Reygers, S.J. Sanders, P. Steinberg, Ann. Rev. Nucl. Part. Sci. **57**, 205 (2007). arXiv:nucl-ex/0701025
50. J. Beringer et al., Particle Data Group, Phys. Rev. D **86**, 010001 (2012). http://pdg.lbl.gov/2013/reviews/contents_sports.html
51. ATLAS Collaboration, ATLAS-CONF-2012-101. http://cds.cern.ch/record/1463915
52. ATLAS Collaboration, ATLAS-CONF-2010-036. http://cds.cern.ch/record/1277675
53. ATLAS Collaboration, ATLAS-CONF-2011-003. http://cds.cern.ch/record/1326960
54. ATLAS Collaboration, Eur. Phys. J. C **72**, 1909 (2012). arXiv:1110.3174
55. ATLAS Collaboration Eur. Phys. J. C (2014). arXiv:1404.2240
56. B. Abelev et al. [ALICE Collaboration], Phys. Rev. Lett. **109**, 112301 (2012). arXiv:1205.6443
57. ATLAS Collaboration, ATLAS-CONF-2013-088. http://cds.cern.ch/record/1580207
58. K. Eskola, H. Paukkunen, C. Salgado, JHEP **0904**, 065 (2009). arXiv:0902.4154
59. LHCb Collaboration, JHEP **1206**, 058 (2012). doi:10.1007/JHEP06(2012)058. arXiv:1204.1620

ATLAS Collaboration

G. Aad[84], B. Abbott[112], J. Abdallah[152], S. Abdel Khalek[116], O. Abdinov[11], R. Aben[106], B. Abi[113], M. Abolins[89], O. S. AbouZeid[159], H. Abramowicz[154], H. Abreu[153], R. Abreu[30], Y. Abulaiti[147a,147b], B. S. Acharya[165a,165b,a], L. Adamczyk[38a], D. L. Adams[25], J. Adelman[177], S. Adomeit[99], T. Adye[130], T. Agatonovic-Jovin[13a], J. A. Aguilar-Saavedra[125a,125f], M. Agustoni[17], S. P. Ahlen[22], F. Ahmadov[64,b], G. Aielli[134a,134b], H. Akerstedt[147a,147b], T. P. A. Åkesson[80], G. Akimoto[156], A. V. Akimov[95], G. L. Alberghi[20a,20b], J. Albert[170], S. Albrand[55], M. J. Alconada Verzini[70], M. Aleksa[30], I. N. Aleksandrov[64], C. Alexa[26a], G. Alexander[154], G. Alexandre[49], T. Alexopoulos[10], M. Alhroob[165a,165c], G. Alimonti[90a], L. Alio[84], J. Alison[31], B. M. M. Allbrooke[18], L. J. Allison[71], P. P. Allport[73], J. Almond[83], A. Aloisio[103a,103b], A. Alonso[36], F. Alonso[70], C. Alpigiani[75], A. Altheimer[35], B. Alvarez Gonzalez[89], M. G. Alviggi[103a,103b], K. Amako[65], Y. Amaral Coutinho[24a], C. Amelung[23], D. Amidei[88], S. P. Amor Dos Santos[125a,125c], A. Amorim[125a,125b], S. Amoroso[48], N. Amram[154], G. Amundsen[23], C. Anastopoulos[140], L. S. Ancu[49], N. Andari[30], T. Andeen[35], C. F. Anders[58b], G. Anders[30], K. J. Anderson[31], A. Andreazza[90a,90b], V. Andrei[58a], X. S. Anduaga[70], S. Angelidakis[9], I. Angelozzi[106], P. Anger[44], A. Angerami[35], F. Anghinolfi[30], A. V. Anisenkov[108], N. Anjos[125a], A. Annovi[47], A. Antonaki[9], M. Antonelli[47], A. Antonov[97], J. Antos[145b], F. Anulli[133a], M. Aoki[65], L. Aperio Bella[18], R. Apolle[119,c], G. Arabidze[89], I. Aracena[144], Y. Arai[65], J. P. Araque[125a], A. T. H. Arce[45], J-F. Arguin[94], S. Argyropoulos[42], M. Arik[19a], A. J. Armbruster[30], O. Arnaez[30], V. Arnal[81], H. Arnold[48], M. Arratia[28], O. Arslan[21], A. Artamonov[96], G. Artoni[23], S. Asai[156], N. Asbah[42], A. Ashkenazi[154], B. Åsman[147a,147b], L. Asquith[6], K. Assamagan[25], R. Astalos[145a], M. Atkinson[166], N. B. Atlay[142], B. Auerbach[6], K. Augsten[127], M. Aurousseau[146b], G. Avolio[30], G. Azuelos[94,d], Y. Azuma[156], M. A. Baak[30], A. Baas[58a], C. Bacci[135a,135b], H. Bachacou[137], K. Bachas[155], M. Backes[30], M. Backhaus[30], J. Backus Mayes[144], E. Badescu[26a], P. Bagiacchi[133a,133b], P. Bagnaia[133a,133b], Y. Bai[33a], T. Bain[35], J. T. Baines[130], O. K. Baker[177], P. Balek[128], T. Balestri[149], F. Balli[137], E. Banas[39], Sw. Banerjee[174], A. A. E. Bannoura[176], V. Bansal[170], H. S. Bansil[18], L. Barak[173], S. P. Baranov[95], E. L. Barberio[87], D. Barberis[50a,50b], M. Barbero[84], T. Barillari[100], M. Barisonzi[176], T. Barklow[144], N. Barlow[28], B. M. Barnett[130], R. M. Barnett[15], Z. Barnovska[5], A. Baroncelli[135a], G. Barone[49], A. J. Barr[119], F. Barreiro[81], J. Barreiro Guimarães da Costa[57], R. Bartoldus[144], A. E. Barton[71], P. Bartos[145a], V. Bartsch[150], A. Bassalat[116], A. Basye[166], R. L. Bates[53], J. R. Batley[28], M. Battaglia[138], M. Battistin[30], F. Bauer[137], H. S. Bawa[144,e], M. D. Beattie[71], T. Beau[79], P. H. Beauchemin[162], R. Beccherle[123a,123b], P. Bechtle[21], H. P. Beck[17], K. Becker[176], S. Becker[99], M. Beckingham[171], C. Becot[116], A. J. Beddall[19c], A. Beddall[19c], S. Bedikian[177], V. A. Bednyakov[64], C. P. Bee[149], L. J. Beemster[106], T. A. Beermann[176], M. Begel[25], K. Behr[119], C. Belanger-Champagne[86], P. J. Bell[49], W. H. Bell[49], G. Bella[154], L. Bellagamba[20a], A. Bellerive[29], M. Bellomo[85], K. Belotskiy[97], O. Beltramello[30], O. Benary[154], D. Benchekroun[136a], K. Bendtz[147a,147b], N. Benekos[166], Y. Benhammou[154], E. Benhar Noccioli[49], J. A. Benitez Garcia[160b], D. P. Benjamin[45], J. R. Bensinger[23], K. Benslama[131], S. Bentvelsen[106], D. Berge[106], E. Bergeaas Kuutmann[16], N. Berger[5], F. Berghaus[170], J. Beringer[15], C. Bernard[22], P. Bernat[77], C. Bernius[78], F. U. Bernlochner[170], T. Berry[76], P. Berta[128], C. Bertella[84], G. Bertoli[147a,147b], F. Bertolucci[123a,123b], C. Bertsche[112], D. Bertsche[112], M. I. Besana[90a], G. J. Besjes[105], O. Bessidskaia[147a,147b], M. Bessner[42], N. Besson[137], C. Betancourt[48], S. Bethke[100], W. Bhimji[46], R. M. Bianchi[124], L. Bianchini[23], M. Bianco[30], O. Biebel[99], S. P. Bieniek[77], K. Bierwagen[54], J. Biesiada[15], M. Biglietti[135a], J. Bilbao De Mendizabal[49], H. Bilokon[47], M. Bindi[54], S. Binet[116], A. Bingul[19c], C. Bini[133a,133b], C. W. Black[151], J. E. Black[144], K. M. Black[22], D. Blackburn[139], R. E. Blair[6], J.-B. Blanchard[137], T. Blazek[145a], I. Bloch[42], C. Blocker[23], W. Blum[82,*], U. Blumenschein[54], G. J. Bobbink[106], V. S. Bobrovnikov[108], S. S. Bocchetta[80], A. Bocci[45], C. Bock[99], C. R. Boddy[119], M. Boehler[48], T. T. Boek[176], J. A. Bogaerts[30], A. G. Bogdanchikov[108], A. Bogouch[91,*], C. Bohm[147a], J. Bohm[126], V. Boisvert[76], T. Bold[38a], V. Boldea[26a], A. S. Boldyrev[98], M. Bomben[79], M. Bona[75], M. Boonekamp[137], A. Borisov[129], G. Borissov[71], M. Borri[83], S. Borroni[42], J. Bortfeldt[99], V. Bortolotto[135a,135b], K. Bos[106], D. Boscherini[20a], M. Bosman[12], H. Boterenbrood[106], J. Boudreau[124], J. Bouffard[2], E. V. Bouhova-Thacker[71], D. Boumediene[34], C. Bourdarios[116], N. Bousson[113], S. Boutouil[136d], A. Boveia[31], J. Boyd[30], I. R. Boyko[64], J. Bracinik[18], A. Brandt[8], G. Brandt[15], O. Brandt[58a], U. Bratzler[157], B. Brau[85], J. E. Brau[115], H. M. Braun[176,*], S. F. Brazzale[165a,165c], B. Brelier[159], K. Brendlinger[121], A. J. Brennan[87], R. Brenner[167], S. Bressler[173], K. Bristow[146c], T. M. Bristow[46], D. Britton[53], F. M. Brochu[28], I. Brock[21], R. Brock[89], C. Bromberg[89], J. Bronner[100], G. Brooijmans[35], T. Brooks[76], W. K. Brooks[32b], J. Brosamer[15], E. Brost[115], J. Brown[55], P. A. Bruckman de Renstrom[39], D. Bruncko[145b], R. Bruneliere[48], S. Brunet[60], A. Bruni[20a], G. Bruni[20a], M. Bruschi[20a], L. Bryngemark[80], T. Buanes[14], Q. Buat[143], F. Bucci[49], P. Buchholz[142], R. M. Buckingham[119], A. G. Buckley[53], S. I. Buda[26a], I. A. Budagov[64], F. Buehrer[48], L. Bugge[118], M. K. Bugge[118], O. Bulekov[97], A. C. Bundock[73], H. Burckhart[30], S. Burdin[73], B. Burghgrave[107], S. Burke[130], I. Burmeister[43], E. Busato[34], D. Büscher[48], V. Büscher[82], P. Bussey[53], C. P. Buszello[167], B. Butler[57], J. M. Butler[22], A. I. Butt[3], C. M. Buttar[53], J. M. Butterworth[77], P. Butti[106], W. Buttinger[28], A. Buzatu[53], M. Byszewski[10],